

# Broad $\text{N}_2\text{H}^+$ emission towards the protostellar shock L1157-B1

C. Codella<sup>1</sup>, S. Viti<sup>2</sup>, C. Ceccarelli<sup>3</sup>, B. Lefloch<sup>3</sup>, M. Benedettini<sup>4</sup>, G. Busquet<sup>4</sup>, P. Caselli<sup>5</sup>,  
F. Fontani<sup>1</sup>, A. Gómez-Ruiz<sup>1</sup>, L. Podio<sup>3</sup>, M. Vasta<sup>1</sup>

Received - ; accepted -

## ABSTRACT

We present the first detection of  $\text{N}_2\text{H}^+$  towards a low-mass protostellar outflow, namely the L1157-B1 shock, at  $\sim 0.1$  pc from the protostellar cocoon. The detection was obtained with the IRAM 30-m antenna. We observed emission at 93 GHz due to the  $J = 1-0$  hyperfine lines. The analysis of the emission coupled with the HIFI CHESS multiline CO observations leads to the conclusion that the observed  $\text{N}_2\text{H}^+(1-0)$  line originates from the dense ( $\geq 10^5 \text{ cm}^{-3}$ ) gas associated with the large ( $20''-25''$ ) cavities opened by the protostellar wind. We find a  $\text{N}_2\text{H}^+$  column density of few  $10^{12} \text{ cm}^{-2}$  corresponding to an abundance of  $(2-8) \times 10^{-9}$ . The  $\text{N}_2\text{H}^+$  abundance can be matched by a model of quiescent gas evolved for more than  $10^4$  yr, i.e. for more than the shock kinematical age ( $\simeq 2000$  yr). Modelling of C-shocks confirms that the abundance of  $\text{N}_2\text{H}^+$  is not increased by the passage of the shock. In summary,  $\text{N}_2\text{H}^+$  is a fossil record of the pre-shock gas, formed when the density of the gas was around  $10^4 \text{ cm}^{-3}$ , and then further compressed and accelerated by the shock.

*Subject headings:* ISM: jets and outflows — ISM: molecules — ISM: abundances

## 1. Introduction

During the first stages of star formation, highly collimated jets from new born stars influence the physical structure of the hosting cloud by sweeping up material, compressing

---

<sup>1</sup>INAF, Osservatorio Astrofisico di Arcetri, Largo Enrico Fermi 5, I-50125 Firenze, Italy  
codella@rcetri.astro.it

<sup>2</sup>Department of Physics and Astronomy, University College London, London, UK

<sup>3</sup>UJF-Grenoble 1 / CNRS-INSU, Institut de Planétologie et d'Astrophysique de Grenoble (IPAG) UMR 5274, Grenoble, F-38041, France

<sup>4</sup>INAF, Istituto di Astrofisica e Planetologia Spaziali, via Fosso del Cavaliere 100, 00133, Roma, Italy

<sup>5</sup>School of Physics and Astronomy, University of Leeds, Leeds LS2 9JT, UK

and accelerating the surrounding environment. The propagation of high velocity outflows generates shock fronts triggering endothermic chemical reactions and ice grain mantle sublimation or sputtering. At a distance of 250 pc (Looney et al. 2007), the chemically rich L1157 bipolar outflow (Bachiller & Pérez Gutiérrez 1997, hereafter BP97, Bachiller et al. 2001) is an ideal laboratory to observe the effects of such shocks on the gas chemistry. L1157 is driven by a low-mass ( $\sim 4 L_{\odot}$ ) Class 0 protostar L1157-mm and it is associated with several blue-shifted (B0, B1, B2) and red-shifted (R0, R1, R2) shocks at different ages (see Fig. 1–Top panel), and seen in both CO (Gueth et al. 1996, 1998), and IR H<sub>2</sub> (e.g. Neufeld et al. 1994, Nisini et al. 2010a). These shocks (see Fig. 1–Bottom panel), when mapped with interferometers, reveal a clumpy bow structure (e.g. Tafalla & Bachiller 1995; Benedettini et al. 2007; Codella et al. 2009) at the apex of different molecular cavities, corresponding to different mass loss episodes (Gueth et al. 1996).

Both interferometer and single-dish surveys confirm that the L1157 outflow is well traced by molecules thought to be released off from the dust mantles such as H<sub>2</sub>CO, CH<sub>3</sub>OH, H<sub>2</sub>O, and NH<sub>3</sub> (e.g. Codella et al. 2010, Lefloch et al. 2010, Vasta et al. 2012) as well as by the refractory grain cores such as SiO (e.g. Nisini et al. 2007; Gusdorf et al. 2008). The abundance of these neutral molecules are enhanced, and the emission shows broad wings (up to 20–30 km s<sup>-1</sup>). On the contrary, diazenylium (N<sub>2</sub>H<sup>+</sup>), usually used as tracer of cold prestellar cores (e.g. Caselli et al. 2002), shows a completely different behaviour. Single-dish (IRAM 30-m) and interferometric (IRAM PdB, SMA, CARMA) observations indicate that N<sub>2</sub>H<sup>+</sup> traces only the central condensation L1157-mm through narrow (0.4–1.0 km s<sup>-1</sup>) emission and it has not been observed, to date, towards the outflow component (Bachiller et al. 2001, Chiang et al. 2010, Tobin et al. 2011, 2012, 2013, Yamaguchi et al. 2012). The interferometric maps show that the narrow N<sub>2</sub>H<sup>+</sup> line traces the protostellar envelope elongated along a direction perpendicular to the outflow axis (i.e. along a hypothetical disk). However, by analysing their IRAM PdB data, Tobin et al. (2011) concluded that although the overall N<sub>2</sub>H<sup>+</sup> velocity structure is unaffected by the outflow, the morphology of the slightly blue-shifted emission ( $|v-v_{sys}| \leq 0.8$  km s<sup>-1</sup>) outlines the outflow cavity walls in the inner 20''–30'' protostellar environment. Tobin et al. (2011) proposed that such emission is due either to outflow entrainment or to a hypothetical shock near the driving protostar. The same suggestion is found in the ATCA N<sub>2</sub>H<sup>+</sup>(1–0) image of the protostellar core CG30 by Chen et al. (2008). On the other hand, Jørgensen et al. (2004) investigated with BIMA the protostellar binary NGC1333-IRAS2A-B at 3mm showing that the spatial distribution of N<sub>2</sub>H<sup>+</sup> peaks towards the nearby starless core IRAS2C, and is missing in the outflows.

Therefore, it is still under debate what role, if any, N<sub>2</sub>H<sup>+</sup> is playing in a shocked gas scenario: Is the N<sub>2</sub>H<sup>+</sup> emission observed by Tobin et al. (2011) and that marks the cavity opened up by the outflow due to just enhanced gas column density or really associated with

a shock? Such question is important, given that  $\text{N}_2\text{H}^+$  is considered a standard molecular tracer of cold and quiescent prestellar environments (e.g. Tafalla et al. 2006).

In order to uniquely answer these questions it is essential to study a region *not* associated with a protostar, as the young (2000 years; Gueth et al. 1996), and bright bow-shock L1157-B1, located at  $\sim 69''$  ( $\sim 0.1$  pc, see Fig. 1) from the protostar. As part of the Herschel<sup>1</sup> Key Program CHESS<sup>2</sup> (Chemical Herschel Surveys of Star forming regions; Ceccarelli et al. 2010), L1157-B1 is currently being investigated with a spectral survey in the  $\sim 80$ – $350$  GHz interval using the IRAM 30-m telescope (Lefloch et al. in preparation), and in the  $\sim 500$ – $2000$  GHz range using the Herschel HIFI instrument (de Graauw et al. 2010). We present here the first unambiguous detection of  $\text{N}_2\text{H}^+$  emission towards a protostellar shock: the observed broad emission has been modeled using a simple pseudo-time dependent chemical model, showing how  $\text{N}_2\text{H}^+$  can be used to shed light on the chemical history of the pre-shock gas.

## 2. Observations and results

The  $\text{N}_2\text{H}^+(1-0)$  line at  $93173.76$  MHz<sup>3</sup> was observed towards L1157-B1 with the IRAM 30-m telescope at Pico Veleta (Spain). The pointed coordinates were  $\alpha_{\text{J2000}} = 20^{\text{h}} 39^{\text{m}} 10^{\text{s}}.2$ ,  $\delta_{\text{J2000}} = +68^\circ 01' 10''.5$ , i.e. at  $\Delta\alpha = +25''.6$  and  $\Delta\delta = -63''.5$  from the driving protostar. The IRAM survey was performed during several runs in 2011 and 2012, using the broad-band EMIR receivers and the FTS spectrometer in its 200 kHz resolution mode, corresponding to a velocity resolution of  $0.6$  km s<sup>-1</sup> at 93.2 GHz. The main-beam efficiency ( $\eta_{\text{mb}}$ ) was 0.75, while the HPBW is  $26''$ . All the spectra are reported here in units of main beam temperature ( $T_{\text{mb}}$ ).

Figure 2 shows the  $\text{N}_2\text{H}^+(1-0)$  spectrum: thanks to the high sensitivity of the IRAM-EMIR receiver (r.m.s. = 2 mK after smoothing the spectrum to  $1.3$  km s<sup>-1</sup>), we are able to detect the three main groups of hyperfine components of the  $J = 1-0$  transition. The integrated intensity is  $327 \pm 14$  mK km s<sup>-1</sup>. The  $\text{N}_2\text{H}^+$  emission in L1157-B1 was hidden in the noise of the BP97 spectrum, which has  $1\sigma$  rms of 20 mK, definitely larger than that of the present dataset (2 mK).

---

<sup>1</sup>Herschel is an ESA space observatory with science instruments provided by European-led principal Investigator consortia and with important participation from NASA.

<sup>2</sup><http://www-laog.obs.ujf-grenoble.fr/heberges/chess/>

<sup>3</sup>It refers to the brightest hyperfine component:  $F_1, F = 2, 3-1, 2$ .

$\text{N}_2\text{H}^+$  is a linear molecular ion in a stable closed-shell  $^1\Sigma$  configuration. The dominant hyperfine interactions are those between the molecular electric field gradient and the electric quadrupole moments of the two nitrogen nuclei (e.g. Caselli et al. 1995), producing a splitting of the  $J = 1-0$  line into 15 hyperfine components, characterised by the corresponding quantum numbers  $F_1$  and  $F$  (e.g. Pagani et al. 2009). To fit the  $\text{N}_2\text{H}^+$  spectrum, we first assumed a unique velocity component and used GILDAS-CLASS90<sup>4</sup>, which gives the best fit (reported in Table 1) of the hyperfine components (see the blue line in Fig. 2–Middle panel). The sum of the opacity at the central velocities of all the hyperfine components  $\sum_i \tau_i$  is  $0.1 \pm 0.9$ . Although the opacity is not well determined the fit indicates  $\sum_i \tau_i \leq 1$ , thus suggesting optically thin emission. Fits fixing  $\tau_i$  to larger values never gave better results.

The peak LSR velocity ( $+1.3 \text{ km s}^{-1}$ ) of the  $\text{N}_2\text{H}^+$  profile is slightly blue-shifted with respect to the ambient velocity ( $+2.6 \text{ km s}^{-1}$ , BP97). The linewidth ( $4.3 \text{ km s}^{-1}$ ) is also considerably larger than what observed by BP97 and Tobin et al. (2013) towards the driving protostar L1157-mm ( $0.6-0.8 \text{ km s}^{-1}$ ). This is clearly shown in Figure 2, where we report the  $\text{N}_2\text{H}^+(1-0)$  line (see the red histogram in the Upper panel) recently observed towards L1157-mm in the framework of the ASAI<sup>5</sup> IRAM 30-m Large program (PI: R. Bachiller & B. Lefloch). The  $\text{N}_2\text{H}^+$  profile from the B1 shock is definitely broader and more blue-shifted than what observed towards the L1157-mm protostar, indicating a different origin. Note also that the weak, but not blended,  $F_1, F = 0, 1-1, 2$  line at  $\sim -8 \text{ km s}^{-1}$  from the main hyperfine component clearly shows blue-shifted emission.

The best fit of Fig. 2 shows a non-negligible residual ( $\sim 3\sigma$ ; see Bottom panel) at about  $-4.0 \text{ km s}^{-1}$ , which suggests non-Gaussian emission from gas at high blue-shifted velocity. Indeed a definitely more satisfactory fit can be obtained by assuming two blue-shifted Gaussian components (see the magenta lines in Fig. 2 and Table 1): (i) a line centered at  $+1.8 \text{ km s}^{-1}$  with  $\text{FWHM} = 2.6 \text{ km s}^{-1}$ , plus (ii) a broader ( $5.9 \text{ km s}^{-1}$ ) line peaking at  $-1.1 \text{ km s}^{-1}$  (dashed and dot-dashed magenta lines in Fig. 2, respectively). In summary, despite the complexity due to the hyperfine components, this clearly shows that a single-Gaussian component is insufficient to reproduce the  $\text{N}_2\text{H}^+(1-0)$  profile towards the B1 shock, and one needs to invoke additional broad blue-shifted emission. The present observation thus reports the first detection of  $\text{N}_2\text{H}^+$  emission towards a low-mass outflow, definitely far from the protostellar environment.

---

<sup>4</sup><http://www.iram.fr/IRAMFR/GILDAS>

<sup>5</sup><http://www.oan.es/asai/>

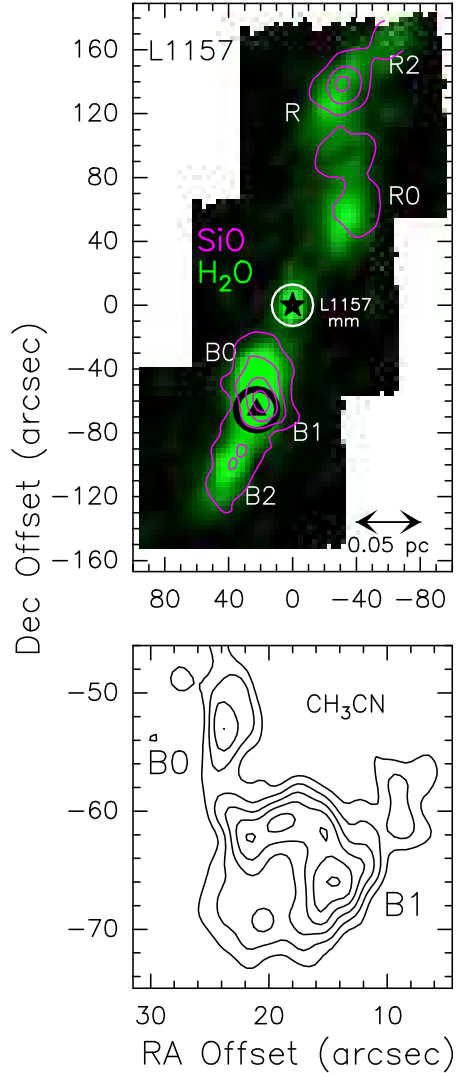


Fig. 1.— *Top panel:* PACS image of L1157 of the integrated  $\text{H}_2\text{O}$  emission at 1669 GHz (Nisini et al. 2010b). Offsets are with respect to the L1157-mm sources (black star), at coordinates:  $\alpha_{\text{J2000}} = 20^{\text{h}} 39^{\text{m}} 06^{\text{s}}.2$ ,  $\delta_{\text{J2000}} = +68^{\circ} 02' 16''.0$ . Magenta contours refer to the  $\text{SiO}(3-2)$  IRAM 30-m map reported by Bachiller et al. (2001). The labels indicate the main blue- and red-shifted knots. Circles are for the IRAM 30-m HPBW at the  $\text{N}_2\text{H}^+(1-0)$  frequency ( $26''$ ), centred at the driving L1157-mm protostar (observed by BP97 and Tobin et al. 2013), and at  $\Delta\alpha = +25''.6$  and  $\Delta\delta = -63''.5$  from the driving protostar (present observations, see black triangles and coordinates reported in Sect. 2). *Bottom panel:* The L1157-B1 bow shock as traced using the  $\text{CH}_3\text{CN}(8-7) K = 0,1,2$  emission at 3 mm, observed with the IRAM PdB interferometer (Codella et al. 2009).

### 3. Physical conditions of the $\text{N}_2\text{H}^+$ gas

The line profiles in L1157-B1, as in other molecular shock spots, have a relatively complex structure where several excitation components are visible. Disentangling such components is not an easy task. In L1157-B1, the recent CO multi-line analysis by Lefloch et al. (2012) indicates that the line profiles are composed by a linear combination of exponential curves  $I_{\text{CO}}(v) = I_{\text{CO}}(0) \exp(-|v/v_0|)$ , independently of the CO transition considered. The three velocity components correspond to three different physical components: (1) a small ( $\sim 7''$ – $10''$ ) dissociative J-type shock called  $g1$  (identified where the line intensity is  $\propto \exp(-|v/12.5|)$ ) dominating at the highest velocities ( $\leq -20 \text{ km s}^{-1}$ ), (2) the outflow cavity walls,  $g2$  ( $\propto \exp(-|v/4.4|)$ ), with size  $\leq 20''$ , and (3) the larger ( $\sim 25''$ ) outflow cavity created by the older bow shock L1157-B2,  $g3$  ( $\propto \exp(-|v/2.5|)$ ) dominating at velocities close to the systemic one ( $v \geq -2 \text{ km s}^{-1}$ ). Each component shows the same slope at all  $J$ , but different relative intensities. The higher is the line excitation the brighter is the  $g1$  component. On the contrary,  $g3$  is observed only towards the low- $J$  ( $\leq 3$ ) CO lines.

Figure 3 compares the  $\text{N}_2\text{H}^+(1-0)$  line with other line profiles observed towards L1157-B1 (Lefloch et al. 2010, Codella et al. 2010, 2012): (i) the CO(16–15) at 1841.3 GHz observed with Herschel-HIFI as an example of a spectrum where the  $g1$  component is clearly dominating the line profile; (ii) the CO(3–2) profile, *as observed towards L1157-B2*, representing a pure  $g3$  profile, without the  $g1$  and  $g2$  components observed towards L1157-B1; (iii) the  $\text{NH}_3(1_0-0_0)$  transition, showing a profile well reproduced by the  $g2$  component alone. The  $\text{N}_2\text{H}^+$  line profile, despite the blending between hyperfine components, seems to exclude the extremely high-velocity emission associated with the  $g1$  component, being consistent with the  $g2$  and  $g3$  ones. In conclusions,  $\text{N}_2\text{H}^+$  is associated either with the B1 outflow cavity (with  $T_{\text{kin}} \simeq 70 \text{ K}$  and  $n_{\text{H}_2} \geq 10^5 \text{ cm}^{-3}$ , according to the LVG CO analysis by Lefloch et al. 2012) and/or with the older and colder B2 cavity ( $\sim 20 \text{ K}$ ,  $\geq 6 \times 10^4 \text{ cm}^{-3}$ ).

The low excitation  $\text{N}_2\text{H}^+(1-0)$  transition ( $E_u = 5 \text{ K}$ ) has a critical density of  $\sim 10^5 \text{ cm}^{-3}$  (e.g. Friesen et al. 2009). The line emission is thus expected to be close to LTE conditions at the densities of the  $g2$  and  $g3$  gas components. Following the results of the LVG analysis by Lefloch et al. (2012), we assume a  $T_{\text{kin}}$  between 20 and 70 K and an emitting size of  $20''$ – $25''$ . The  $\text{N}_2\text{H}^+$  total column density is then well constrained  $N(\text{N}_2\text{H}^+) = (2-8) \times 10^{12} \text{ cm}^{-2}$ . Using the source-averaged column density  $N(\text{CO}) = 1 \times 10^{17} \text{ cm}^{-2}$  (found for both  $g2$  and  $g3$  by Lefloch et al. 2012), and assuming  $[\text{CO}]/[\text{H}_2]=10^{-4}$ , we can derive the  $\text{N}_2\text{H}^+$  abundance:  $X(\text{N}_2\text{H}^+) = 2-8 \times 10^{-9}$ . A lower abundance, between  $4 \times 10^{-10}$  and  $\sim 10^{-9}$ , is derived for the weaker emission at higher velocity, represented by the velocity component peaking at  $-1.1 \text{ km s}^{-1}$  (see Table 1).

These values are consistent with what found towards the L1157-mm protostar by BP97

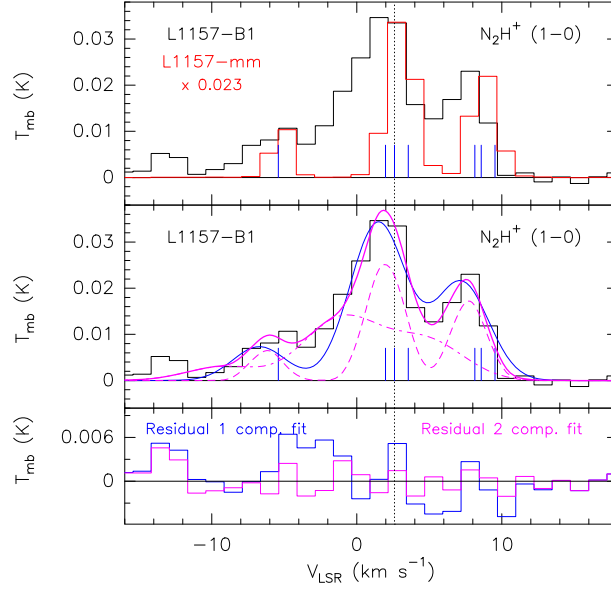


Fig. 2.— *Upper panel*:  $\text{N}_2\text{H}^+(1-0)$  line (black histogram; in  $T_{\text{mb}}$  scale) observed in L1157-B1 with the IRAM 30-m antenna. The red histogram refers to the  $\text{N}_2\text{H}^+(1-0)$  spectrum (scaled for a direct comparison) as observed towards L1157-mm with the IRAM 30-m antenna in the framework of the ASAI IRAM Large Program (PI: R. Bachiller & B. Lefloch). The vertical dashed line indicates the ambient LSR velocity ( $+2.6 \text{ km s}^{-1}$ , from BP97). The vertical seven blue lines stand for the 15 hyperfine components of the  $\text{N}_2\text{H}^+(1-0)$  pattern (several of them spectrally unresolved at the present frequency resolution; see Pagani et al. 2009). We centered the spectrum at the frequency of the main hyperfine component  $F_1, F = 2, 3-1, 2$  (93173.76 MHz). *Middle panel*: Analysis of the  $\text{N}_2\text{H}^+(1-0)$  profile. The blue line shows the best fit (FWHM =  $4.3 \text{ km s}^{-1}$ ) assuming a single Gaussian component. The magenta solid line shows the best fit using two Gaussian components (dashed magenta: FWHM =  $2.6 \text{ km s}^{-1}$ ; dot-dashed magenta: FWHM =  $5.9 \text{ km s}^{-1}$ ) in order to minimise the residual. The corresponding residuals are reported in the *Bottom panel*: the single component approach gives a  $3\sigma$  (rms = 2 mK) residual.

Table 1: Parameters of the hyperfine fits to the  $\text{N}_2\text{H}^+(1-0)^a$  line, and total column density.

$T_{\text{peak}}$ (mK)	rms (mK)	$V_{\text{peak}}$ (km s $^{-1}$ )	$FWHM$ (km s $^{-1}$ )	$\sum_i \tau_i$	$N_{\text{tot}}^c$ (cm $^{-2}$ )
1 component fit					
34(2)	2	+1.3(0.1)	4.3(0.2)	0.1(0.9)	2.4–7.8 $10^{12}$
2 components fit					
26(2)	2	+1.8(0.1)	2.6(0.1)	0.2(0.2)	2.4–8.0 $10^{12}$
14(2)	2	–1.1(0.4)	5.9(0.9)	0.1(0.1)	0.4–1.3 $10^{12}$

<sup>a</sup> The spectrum has been centered at the frequency of the main hyperfine component  $F_1, F = 2, 3-1, 2$  (93173.76). Frequencies have been extracted from the Cologne Database of Molecular Spectroscopy (Müller et al. 2005). See also Pagani et al. (2009). <sup>b</sup> At a spectral resolution of 1.3 km s $^{-1}$ . <sup>c</sup> Assuming a  $T_{\text{kin}} = 20\text{--}80$  K and a source size of 20''–25'' (see text).

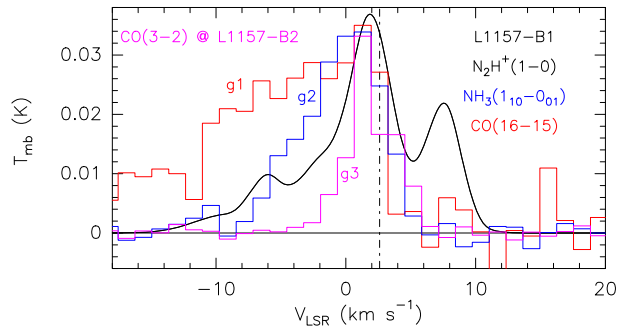


Fig. 3.— Comparison of the  $\text{N}_2\text{H}^+(1-0)$  fit (black; see Fig. 2) with typical profiles of the  $g1$ ,  $g2$ , and  $g3$  components (from Codella et al. 2010, and Lefloch et al. 2012, see text).  $\text{CO}(16-15)$  represents  $g1$  (1841.3 GHz, red, decreased by a factor 6.4 for a direct comparison), while  $\text{NH}_3(1_0-0_0)$  (572.5 GHz, blue, decreased by a factor 4.5) is for  $g2$ . In addition, we report the  $\text{CO}(3-2)$  spectra for  $g3$  (magenta, 345.8 GHz, decreased by a factor 269.0) observed by Lefloch et al. (2012) towards the L1157-B2 position, tracing a cavity older than the L1157-B1 one, and created by a previous wind ejection (Gueth et al. 1996). The spectra have been smoothed to a common spectral resolution of 1.3 km s $^{-1}$ .



( $4 \times 10^{-9}$ ) using the IRAM 30-m antenna. On the other hand, Chiang et al. (2010) measured lower values ( $3\text{--}6 \times 10^{-10}$ ) towards L1157-mm using the CARMA array, possibly due to interferometric filtering. Similar values have been also found in CO depleted prestellar cores and dense protostellar envelopes ( $\sim 10^{-10}\text{--}10^{-9}$ ; see e.g. Caselli et al. 2002, Tafalla et al. 2004, 2006, Maret et al. 2007, Chen et al. 2007, 2008). This value represents an estimate of the abundance of the gas in the outflow cavities and will be used for a comparison with the outputs predicted by our models.

#### 4. $\text{N}_2\text{H}^+$ chemistry in L1157-B1

To understand the origin of the observed  $\text{N}_2\text{H}^+$ , we compared its measured abundance with the  $\text{N}_2\text{H}^+$  abundance predicted by a simple pseudo-time dependent model. We used the publicly available ASTROCHEM code<sup>6</sup>. The code follows the evolution of the chemical composition of a gas cloud initially in the diffuse state and with fixed temperature and density. A simple gas-grain interaction due to freeze-out, thermal, and photo-desorption, has been considered. In these calculations we assumed a nitrogen elemental abundance equal to  $2.1 \times 10^{-5}$  (with respect to H nuclei), carbon and oxygen equal to  $7.3 \times 10^{-5}$  and  $1.8 \times 10^{-4}$  respectively, grain size of  $0.1 \mu\text{m}$ , and cosmic ionisation rates  $\zeta$  in the  $10^{-17}\text{--}10^{-16} \text{ s}^{-1}$  range (e.g. Dalgarno 2006; Padovani et al. 2009).

Figure 4 shows the predicted  $\text{N}_2\text{H}^+$  abundance as a function of the volume density at different evolutionary times, from  $2 \times 10^3 \text{ yr}$  (the age of L1157-B1) to  $1 \times 10^7 \text{ yr}$ . The chemistry of  $\text{N}_2\text{H}^+$  is relatively simple: it is formed by the reaction of the  $\text{H}_3^+$  (created by the cosmic rate ionisation of  $\text{H}_2$ ) and destroyed by the reaction of CO (or electrons in case of CO depletion). Therefore, the larger the density the lower is the  $\text{H}_3^+$  abundance, and consequently  $X(\text{N}_2\text{H}^+)$ . The comparison of the measured and predicted  $\text{N}_2\text{H}^+$  abundances yields an important conclusion: the observed  $\text{N}_2\text{H}^+$  abundance is perfectly matched by a model of cold, quiescent, and relatively old ( $\geq 10^4 \text{ yr}$ ) gas and does not require the intervent of a shock. The age of the shock in L1157-B1 is around 2000 yr (Gueth et al. 1996); hence Fig. 4 shows that  $\text{N}_2\text{H}^+$  was present before the shock occurred, and it is consistent with a pre-shock  $\text{H}_2$  density of  $\leq 5 \times 10^5 \text{ cm}^{-3}$ . In addition, given that  $X(\text{e}) \propto n_{\text{H}_2}^{-1/2}$  (e.g. McKee 1989), we can *speculate* that the lower  $X(\text{N}_2\text{H}^+)$  abundance (by a factor  $\simeq 5\text{--}6$ ) measured at the highest velocities indicates a density gradient in the shocked gas in the cavity. In other words, the  $\text{N}_2\text{H}^+$  emitting at higher velocities could trace gas with  $n_{\text{H}_2}$  about one order of magnitude higher than that of the gas at velocities closer to the systemic one.

---

<sup>6</sup><http://smaret.github.com/astrochem/>

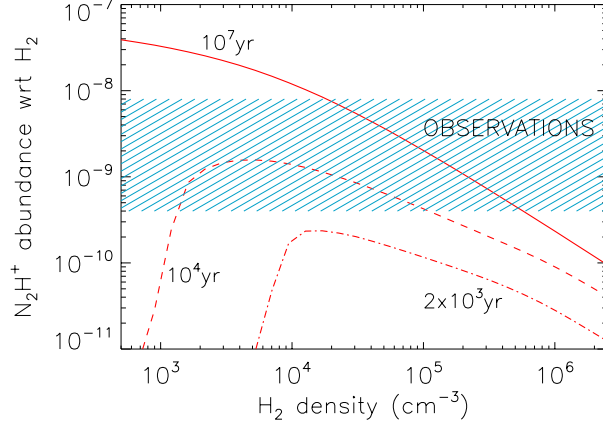


Fig. 4.—  $\text{N}_2\text{H}^+$  abundance, with respect to  $\text{H}_2$ , versus the  $\text{H}_2$  density at different times: from  $2 \times 10^3$  yr (the age of L1157-B1) to  $1 \times 10^7$  yr. The dashed blue box gives the observed value with the  $1 \sigma$  uncertainty (see text). The gas is at a temperature of 70 K, but the curve is identical in the range 20 to 70 K. The cosmic ionisation rate is  $10^{-16} \text{ s}^{-1}$ .

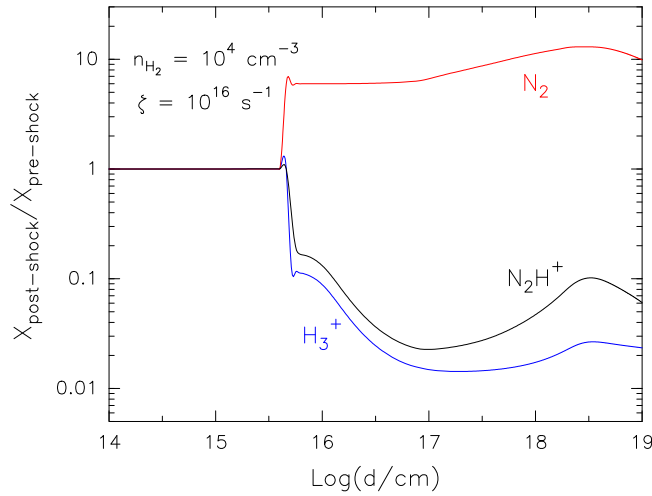


Fig. 5.— Example of UCL\_CHEM model (Viti et al. 2004) showing how the fractional abundances (with respect to  $\text{H}_2$ ) of  $\text{N}_2\text{H}^+$ ,  $\text{H}_3^+$ , and  $\text{N}_2$  can vary as a function of distance (see text).

In addition, to verify whether the detected  $\text{N}_2\text{H}^+$  molecules were pre-existing to the shock, we used a shock model of L1157-B1 reported by Viti et al. (2011), who coupled the chemical model UCL\_CHEM with a parametric shock model (Jiménez-Serra et al. 2008). UCL\_CHEM is a gas-grain chemical code which first simulates the formation of high-density clumps from an atomic diffuse cloud, and then follows their chemical evolution when subjected to the passage of a C-type shock. Full details of the code can be found in Viti et al. (2004, 2011). We updated the grid of models from Viti et al. (2011) varying the cosmic ray ionisation rate  $\zeta$  (which of course directly influences the behaviour of ions) in the  $10^{-17}$ – $10^{-16}$   $\text{s}^{-1}$  range. Figure 5 reports an example of a UCL\_CHEM shock model assuming  $\zeta = 10^{-16}$   $\text{s}^{-1}$  and a pre-shock density of  $10^4$   $\text{cm}^{-3}$ . We confirm that  $\text{N}_2\text{H}^+$  is indeed formed in the gas phase and that the passage of a shock, with the subsequent release of  $\text{N}_2$  into the gas, does not yield an increase in the  $\text{N}_2\text{H}^+$  abundance. This is consistent with the lack of signatures of very high-velocity associated with the  $g1$  component in the  $\text{N}_2\text{H}^+(1-0)$  profile. On the contrary, the passage of a shock does decrease the  $\text{N}_2\text{H}^+$  abundance by about 1–2 orders of magnitude, depending on the pre-shock conditions and velocity of the shock. This allows us to further constrain the pre-shock density to  $\sim 10^4$   $\text{cm}^{-3}$  (see Fig. 4) in order to maintain the observed abundance once the outflow cavities have been compressed to  $\geq 10^5$   $\text{cm}^{-3}$ . A value of  $\zeta$  ( $\sim 10^{-16}$   $\text{s}^{-1}$ ) helps to achieve and maintain a high  $\text{N}_2\text{H}^+$  abundance. A pre-shock density of  $\sim 10^4$   $\text{cm}^{-3}$  is consistent with the results suggested by the study of deuteration in L1157-B1 (Codella et al. 2012b) where it was found that the most likely scenario is that of a gas passing through a pre-shock phase with  $n_{\text{H}_2} \leq 4 \times 10^4$   $\text{cm}^{-3}$ , during which formaldehyde and methanol ices are formed.

## 5. Conclusions

We present the first detection of diazenylium towards outflowing gas far from the driven low-mass protostar. We found evidence that  $\text{N}_2\text{H}^+(1-0)$  emission observed towards the L1157-B1 shock originates from the dense ( $\geq 10^5$   $\text{cm}^{-3}$ ) gas associated with the cavities opened, and accelerated by the prototellar wind. The line width ( $\geq 4$   $\text{km s}^{-1}$ ) is significantly broader than the  $\text{N}_2\text{H}^+$  line widths previously observed towards the driving protostar L1157-mm ( $\leq 1$   $\text{km s}^{-1}$ ), as well as than the typical line widths observed in quiescent regions, probably as a result of the energy injection from the sweeping outflow. The estimated  $\text{N}_2\text{H}^+$  abundance is  $(2-8) \times 10^{-9}$ , which can be reproduced by a model of quiescent gas evolved for more than  $10^4$  yr (i.e. older than the shock kinematical age, 2000 yr). In other words,  $\text{N}_2\text{H}^+$  can be considered a fossil record of the pre-shock phase, when the gas density was  $\sim 10^4$   $\text{cm}^{-3}$ . Modelling of C-shocks confirms that  $X(\text{N}_2\text{H}^+)$  is not enhanced by the passage of the shock. The present  $\text{N}_2\text{H}^+$  detection is the result of the increase of its column density due to

the compression (by a factor  $\sim 10$ ) of swept-up material, and not to its relative abundance.

C. Codella, C. Ceccarelli, B. Lefloch, and S. Viti acknowledge the financial support from the COST Action CM0805 “The Chemical Cosmos”. The Italian authors gratefully acknowledge funding from Italian Space Agency (ASI) through the contract I/005/011/0, which also supports the fellowships of G. Busquet and A. Gómez-Ruiz. C. Ceccarelli and B. Lefloch acknowledge funding from the French Space Agency CNES and the National Research Agency funded project FORCOM, ANR-08-BLAN-0225. S. Viti acknowledges support from the [European Community’s] Seventh Framework Programme [FP7/2007-2013] under grant agreement n° 238258.

## References

- Bachiller R., Pérez Gutiérrez M., Kumar M. S. N., et al., 2001, *A&A* 372, 899  
Bachiller R., & Pérez Gutiérrez M., 1999, *ApJ* 487, L93 (BP97)  
Benedettini M., Viti S., Codella C., et al., 2007, *MNRAS* 381, 1127  
Caselli P., Myers P.C., Thaddeus P., 1995, *ApJ* 455, L77  
Caselli P., Benson P.J., Myers P. C., Tafalla M., 2002, *ApJ* 572, 238  
Ceccarelli C., Bacmann A., Boogert A., et al., 2010, *A&A* 521, L22  
Chen X., Launhardt R., Bourke T.L., Henning Th., Barnes P.J., 2008, *ApJ* 683, 862  
Chen X., Launhardt R., Henning Th., 2007, *ApJ* 669, 1058  
Chiang H.-F., Looney L.W., Tobin J.J., & Hartmann L., 2010, *ApJ* 709, 470  
Codella C., Benedettini M., Beltrán M.T., et al. 2009, *A&A* 507, L25  
Codella C., Lefloch B., Ceccarelli C., et al., 2010, *A&A* 518, L112  
Codella C., Ceccarelli C., Bottinelli S., et al., 2012a, *ApJ* 744, L164  
Codella C., Ceccarelli C., Lefloch B., et al., 2012b, *ApJ* 757, L9  
Dalgarno A., 2006, *Proceedings of the National Academy of Science* 103, 12269  
Friesen R.K., Di Francesco J., Shirley Y.L., Myers P.C., 2009, *ApJ* 697, 1457  
de Graauw Th., Helmich F.P., Phillips T.G., et al., 2010, *A&A* 518, L6  
Gusdorf A., Pineau des Forêts G., Cabrit S., Flower D.R., 2008, *A&A* 490, 695  
Gueth F., Guilloteau S., & Bachiller R., 1996, *A&A* 307, 891  
Gueth F., Guilloteau S., & Bachiller R., 1998, *A&A* 333, 287  
Jiménez-Serra I., Caselli P., Martín-Pintado J., Hartquist T.W., 2008, *A&A* 482, 549  
Jørgensen J.K., Hogerheijde M.R., van Dishoeck E.F., Blake G.A., Schöier F.L., 2004, *A&A* 413, 993  
Lefloch B., Cabrit S., Codella C., et al., 2010, *A&A* 518, L113  
Lefloch B., Cabrit S., Busquet G., et al., 2012, *ApJ* 757, L25

- Looney L. W., Tobin J., & Kwon W., 2007, *ApJ* 670, L131
- Maret S., Bergin E.A., & Lada C.J., 2007, *ApJ* 670, L25
- McKee, C.F., 1989, *ApJ* 345, 782
- Müller H.S.P., Schöier F.L., Stutzki J., Winnewisser G., 2005, *J.Mol.Struct.* 742, 215
- Neufeld D.A., & Green S., 1994, *ApJ* 432, 158
- Nisini B., Codella C., Giannini T., et al., 2007, *A&A* 462, 163
- Nisini B., Giannini T., Neufeld D.A., et al., 2010a, *ApJ* 724, 69
- Nisini B., Benedettini M., Codella C., et al., 2010b, *A&A* 518, L12
- Padovani M., Galli D., & Glassgold A.E., 2009, *A&A* 501, 619
- Pagani L., Daniel F., & Dubernet M.-L., 2009, *A&A* 494, 719
- Tafalla M., & Bachiller R., 1995, *ApJ* 443, L37
- Tafalla M., Myers P.C., Caselli P., Walmsley C.M., 2004, *A&A* 416, 191
- Tafalla M., Santiago-García J., Myers P.C., et al., 2006, *A&A* 455, 577
- Tobin J.J., Hartmann L., Chiang H.-F., et al., 2011, *ApJ* 740, 45
- Tobin J.J., Hartmann L., Bergin E., et al., 2012, *ApJ* 748, 16
- Tobin J.J., Bergin E., Hartmann L., et al., 2013, *ApJ* 765, 18
- Wilson T.L., & Rood R., 1994, *ARA&A* 32, 191
- Vasta, M., Codella, C., Lorenzani, A., et al., 2012, *A&A* 537, A98
- Viti S., Collongs M.P., Dever J.W., McCoustra M.R.S., Williams D.A., 2004, *MNRAS* 354, 1141
- Viti S., Jiménez-Serra I., Yates J.A., et al., 2011, *ApJ* 740, L3 Yamaguchi T., Takano S., Watanabe Y., et al., 2012, *PASP* 64, 105